European Research Infrastructure supporting Smart Grid and Smart Energy Systems Research, Technology Development, Validation and Roll Out – Second Edition

Project Acronym: **ERIGrid 2.0**

Project Number: **870620**

Technical Report Lab Access User Project

Study of innovative impedance-based stability analysis for the power systems composed of inverter-based resources (ISAIPS –Impedance-based Stability Analysis on Inverter-based Power Systems)

Access Duration: 23 February 2023 to 18 March 2023

Report Information

Document Administrative Information	
Project Acronym:	ERIGrid 2.0
Project Number:	870620
Access Project Number:	157
Access Project Acronym:	ISAIPS
Access Project Name:	Study of innovative impedance-based stability analysis for the power systems composed of inverter-based resources
User Group Leader:	Yuko Hirase (Toyo University)
Document Identifier:	ERIGrid2-Report-Lab-Access-User-Project-ISAIPS-draft-v1.0
Report Version:	V1.0
Contractual Date:	27/12/22
Report Submission Date:	31/3/23
Lead Author(s):	Yuko Hirase (Toyo University)
Co-author(s):	Kazuki Ohuchi (Toyo University), Tomoya Ide (Toyo University)
Keywords:	Impedance, Inverter, Control, Power System, Stability, European Union (EU), H2020, Project, ERIGrid 2.0, GA 870620
Status:	Draft

Change Log

Date	Version	Author/Editor	Summary of Changes Made
31/3/23	v1.0	Yuko Hirase (Toyo University)	Draft report
14/4/23	V1.1	Yuko Hirase (Toyo University)	Figure 21 is changed.

Table of Contents

List of Figures

List of Tables

List of Abbreviations

BTB	**Back-to-Back**
CO	**Project Coordinator**
DFT	**Discrete Fourier Transformation.**
EC	**European Commission**
GFL	**Grid-Following**
GFM	**Grid-Forming**
HIL	**Hardware in the Loop**
HTD	**Holistic Test Description**
LA	**Lab Access**
MG	**Microgrid**
SCADA	**Supervisory Control and Data Acquisition**
SCR	**Short Circuit Ratio**
S/N	**Signal to Noise**
UG	**User Group**
UP	**User Project**
VSM	**Virtual Synchronous Machine**

Executive Summary

1. Summary

The objective of this research is to analyse and control the impedance of distributed power supplies connected via power electronic (power electronics) devices and to prevent accidents caused by power system resonance phenomena. A laboratory-scale real micro grid (MG) will be constructed, and various constraints for impedance measurement will be clarified to establish procedures and methods. Furthermore, we will obtain guidelines on the amount of power supply impedance required for grid stabilization and robustness. This will enable power supply manufacturers and transmission/distribution companies to promptly enter the market and start operation by utilizing the results of this research when regulations on impedance analysis are introduced in the future.

2. Lab-Access User Project Information

User Project Acronym	ISAIPS – Impedance-based Stability Analysis on Inverter-based Power Systems
User Project Title	Study of innovative impedance-based stability analysis for the power systems composed of inverter-based resources
Main Scientific/Technical Field	Power electronics
Host infrastructure	National Smart Grid Laboratory (SINTEF, Norway)
Access period	From 20.2.23 to 18.3.23 (24 days)
Leader of the user group	Yuko Hirase (Assoc. professor, Toyo University, Japan)
Member of the user group (1)	Kazuki Ohuchi (Student, Toyo University, Japan)
Member of the user group (2)	Tomoya Ide (Student, Toyo University, Japan)

3. State-of-the-Art/State-of-Technology

To realize a carbon-neutral and decarbonized society, the spread of power sources derived from renewable energy sources is expanding. Unlike conventional synchronous generators, power electronics devices called grid-connected inverters, which are used to connect renewable energy sources to a power system, have high-speed and complex controls. Therefore, it is necessary to accurately measure and control the impact of power electronics devices on the power system. However, it is difficult to use conventional linear mathematical model-based methods because power electronics devices developed by each manufacturer are black boxes whose specifications are not disclosed to the public. Therefore, research on impedance-based analysis has been attracting attention as an alternative method. Impedance-based analysis is a method of data-driven analysis that enables analysis using only measurement data, even when devices with black box control are connected. The keys are how accurately to obtain huge amounts of data and how widely to analyse data over a wide frequency bandwidth.

4. Executed Tests and Experiments

1. Pre-process

The high-performance voltage source existing in the laboratory has multiple output ports and was used to both simulate an infinite bus in the target system and to amplify the power of the perturbed signal. Each perturbation signal was continuously injected for a sufficient settling time (3 cycles or 3 seconds).

All equipment in the laboratory can be controlled and measured by a SCADA (Supervisory Control and Data Acquisition) called RT-LAB, which can be programmed to inject perturbation signals of 100 to 200 (depends on the complexity of the system) frequencies in sequence in the 0.5 Hz to 2 kHz bandwidth. This process was prepared with the cooperation of the host.

2. Experiments

To measure the voltages/currents by injecting a perturbation signal into the test object. The injecting a perturbation was conducted in three phases.

Step 1: Connected the converter to the existing constant voltage source (EGSTON) and measured the voltage/current of the converter alone. The objective was to determine the minimum amount of perturbation signal for which the impedance can be calculated.

Step 2: The system under test was split and perturbation signals were injected at the split points. To input the voltage perturbation, transformers existing in the laboratory were modified to the desired winding ratios and connected in series to the split points. The voltage amplitude was determined such that not only were there sufficient signal strengths, but also that magnetic saturation of the transformer did not occur.

Step 3: Voltages/currents were measured by changing the strength of the constant voltage source and the converter's operating mode.

3. Post-process

The measured voltages and currents on stationary reference frames were converted off-line to signals on synchronous reference frames and further converted to complex numbers using the discrete Fourier transform (DFT). Because the target system is three-phase AC, the resulting voltage and current were both matrices with 2x2 complex elements. From these, the impedance matrices on the left and right sides of the perturbation injection point were calculated respectively, and the loop gain matrix was calculated using these matrices. Nyquist's stability theorem was applied to all eigenvalues of the loop gain matrix to determine the stability of the system.

5. Results and Conclusions

An experimental environment for impedance-based stability analysis using a transformer-based voltage perturbation injection method was established, and reasonable stability results were successfully obtained. The experimental analysis over a wide bandwidth is an unprecedented success. It was not possible to make various changes to the hardware configuration and software parameters in 24 days, a follow-up test should be planned.

6. Open Issues and Suggestions for Improvements

Thanks to the generosity and hospitality of the host, a very meaningful and delightful experience were obtained. No major improvements were needed, except we would like to see the cost coverage expanded for future programs.

1 Lab-Access User Project Information

1.1 Overview

USER PROJECT PROPOSAL

User Project Acronym	ISAIPS – Impedance-based Stability Analysis on Inverter-based Power Systems
User Project Title	Study of innovative impedance-based stability analysis for the power systems composed of inverter-based resources
Main Scientific/Technical Field	Power electronics
Keywords (5 max., free text)	impedance, inverter, control, power system, stability

HOST LABORATORY/RESEARCH INFRASTRUCTURE

Host infrastructure	National Smart Grid Laboratory (SINTEF)
Starting date of the access	20.2.23
Access period	24 days

LEADER OF THE USER GROUP

Name	Yuko Hirase
Nationality	Japan
Gender	Female
Age below 35-year-old (Y/N)?	N
Email address	hirase028@toyo.jp
Organization name	Toyo University
Organization address	2100, Kujirai, Kawagoe, Saitama 350-8585, Japan
Organization website	https://www.toyo.ac.jp/en/
Organization activity type	UNI - University and other higher education organizations

MEMBERS OF THE USER GROUP

Name	Kazuki Ohuchi
Nationality	Japan
Gender	Male
Age below 35-year-old (Y/N)?	Y
Email address	s36C02100012@toyo.jp
Organization name	Toyo University
Organization address	2100, Kujirai, Kawagoe, Saitama 350-8585, Japan
Organization website	https://www.toyo.ac.jp/en/
Organization activity type	UNI - University and other higher education organizations

Name	Tomoya Ide
Nationality	Japan
Gender	Male
Age below 35-year-old (Y/N)?	Y
Email address	s16C02001098@toyo.jp
Organization name	Toyo University
Organization address	2100, Kujirai, Kawagoe, Saitama 350-8585, Japan
Organization website	https://www.toyo.ac.jp/en/
Organization activity type	UNI - University and other higher education organizations

1.2 Research Motivation, Objectives, and Scope

The objective of this research is to obtain experimental results to validate the results of pre-liminary studies based on mathematical theory and numerical simulations of impedance-based power converter analysis and control methods. Specifically, a new data-driven grid stability analysis method will be demonstrated using impedances measured in actual test facilities. The objective of this method is to improve the fault tolerance of power systems by accurately predicting the impact of disturbances caused by power electronics equipment on power system stability and improving its dynamic characteristics. Even if many power electronics devices, which lead to the complexity, are connected to the modern power systems, the intellectual property of equipment manufacturers and power transmission and distribution companies will be protected.

On the other hand, many power-electronic devices are equipped with advanced control methods that actively stabilize the power system, such as a Virtual Synchronous Machine (VSM) control. Power systems to which many such advanced control devices are connected have resonance points in various frequency bands, and more accurate impedance measurement is required. Therefore, one of the objectives of this project is to reproduce such a recent power system more faithfully on a laboratory scale and to clarify the empirical limits of impedance-based analysis.

The author is the leader of the project and two students from her laboratory will participate as research collaborators. The start date is February 23, 2023. During the approximately seven months between the start of the project, continued discussions with SINTEF in online meetings were held discussing about the objectives of the project and the feasibility the experimental tests. Based on this, the measured data during the access period will be compared with existing results based on mathematical theory and numerical simulations to evaluate the validity of the test results.

1.3 Structure of the Document

This document is organised as follows: Section 2 briefly outlines the state-of-the-art/state-of-technology that provides the basis of the realised Lab Access (LA) User Project (UP). Section 3 briefly outlines the performed experiments whereas Section 4 summarises the results and conclusions. Potential open issues and suggestions for improvements are discussed in Section 5. Finally, Laboratory Access photos and videos provided in the Appendix A.

2   State-of-the-Art/State-of-Technology

The impedance-based power system stability analysis method was first used by R. D. Middlebrook in 1976 to evaluate the dynamic interaction between a DC power supply and its electromagnetic input filter of a converter [Middlebrook Cuk, 1976]. In 1997, M. Belkhayat extended the above theory from DC system to a three-phase AC system transformed on a dq-synchronous frame [Belkhayat, 1997]. In this method, the impedance on a three-phase AC system is represented by a 2x2 matrix called dq impedance, so stability analysis based on the Nyquist criterion like scalar impedance is not possible. As an approach to solve this problem, a sequence impedance different from dq impedance was presented by J. Sun in 2009 [Sun, 2009] and A. Rygg and M. Molinas, etc in most recent research [Rygg, Molinas, Unamuno, Zhang, Cai, 2017]. M. Molinas and M. Amin have published extensively on impedance-based stability evaluation methods and non-stationary signal analysis [Rygg, Molinas, Unamuno, Zhang, Cai, 2017], [Amin Molinas, 2016], [Amin Molinas, 2017], [Rygg, Molinas, Zhang, Cai, 2017]. J. A. Suul, S. D'Arco, etc have also presented the results of demonstration tests on the virtual synchronous machine-based control applying for the vehicle-to-grid services [Suul, D'Arco, Guidi, 2016]. Meanwhile, in Japan, T. Kiribuchi presented an impedance-based stability analysis of servo-driven DC power feeding systems in 2019 [Kiribuchi, Zaitsu, Doi, Kusaka, Itoh, 2019], while an impedance-based analysis applied to a large-scale AC system including power electronics equipment with VSG-based control was first presented by the proposers at the International Power Electronics Conference (IPEC 2022 ECCE Asia) in 2022 [Ohuchi, Hirase, Molinas, 2022].

Recent examples [Shah, Koralewicz, Gevorgian, Liu, Fu, 2021] of the application of impedance-based methods to stability analysis include the high-voltage direct current (HVDC) transmission systems at State Grid Corporation in China and the Xcel system in the USA, the solar power plant at the National Renewable Energy Laboratory (NREL) in the USA, and the offshore wind farms in Hornsey, UK and BorWin1 power plant in Germany. These projects require stability analysis in the planning and development stages. However, in multi-vendor systems involving multiple distributors (vendors), such as the HVDC transmission offshore wind power generation systems in Europe, for example, prior stability analysis is difficult because the intellectual property of each manufacturer involved in development is usually not disclosed. On the other hand, with impedance-based system stability analysis, it is possible to perform stability analysis of a large-scale system even in the planning and development stages by using a combination of black-box models from each manufacturer.

In conventional impedance-based analysis, however, the entire circuit is separated at the device (load or power supply) connection node into the device side and the system side, and the interaction is evaluated by treating the impedance ratio of each as equivalent to the open loop gain of a control system negative feedback loop. However, it cannot be applied to loop or mesh circuits, where it is difficult to separate the entire circuit into two parts without performing some form of aggregation. Therefore, in the proposed impedance-based analysis, black box power and load circuits that are arbitrarily added to transmission and distribution lines are added to existing circuits according to simple rules, regardless of the manufacturer of each device, components (devices, transmission, and distribution networks), device connection locations, and inverter control, and the entire system is analysed as one large impedance (admittance). This makes it possible to easily analyse the presence or absence of dynamic instability factors in the entire system without dividing the circuit, even in complex loop or mesh power systems containing black-boxed intellectual property information. In other words, it leads to the construction of power systems with a high degree of freedom and scalability.

Furthermore, the capacitive components such as the ground capacitance of π transmission lines, capacitor banks, and inverter output filter capacitors, which were often omitted in previous studies due to the complexity of the mathematical model, will be included in the analysis to cover large-scale power systems that are closer to reality. In addition, as an advanced grid forming type (GFM) inverter control that contributes to grid stabilization more than grid following type (GFL) inverter control, VSG control will be included in the power electronics equipment to clarify the range of adjustable impedance. This will contribute to the spread of renewable energy interconnected by inverters.

3 Executed Tests and Experiments

3.1 Test Plan, Standards, Procedures, and Methodology

3.1.1. Test plan

Step 1:

First, check to see if a sufficient signal-to-noise (S/N) ratio is obtained to calculate the impedance. By Fourier transforming the perturbed signal directly superimposed on the signal on the rotating frame, only the perturbed frequency signal component is extracted from the reference signal. Therefore, the amplitude of the measurement signal need not exactly match the injected one, but the signal accuracy will be reduced if the noise ratio is relatively large. On the other hand, if the ratio of perturbed S/N ratio is set too large beforehand, the stability analysis perspective for small signal analysis around the equilibrium point is lost and the calculation results become meaningless. Therefore, the objective of this stage is to determine the minimum amount of perturbation signal for which the impedance can be calculated. In this stage, the impedance of the converter alone can be obtained.

Step 2:

The entire system is separated into two sub-systems, and the loop gain is calculated from the load and source impedances at the separation point. A perturbation voltage of the magnitude determined in Step 1 is input on the primary side and the secondary side of a voltage transformer is inserted in series at the separation point. Since magnetic saturation of the transformer will be a problem in the low frequency region of the perturbation frequency, the voltage amplitude must be sufficiently small as the frequency decreases. That is, the goal is to estimate the lowest detectable frequency and the smallest voltage.

In this phase, the load side is assumed to be a bidirectional grid-connected inverter with grid-GFL or GFM control. On the other hand, the source side of the secondary transformer is assumed to be an infinite bus (i.e., a constant voltage source) and unaffected by the input perturbations. Therefore, the purpose of this stage is to create an experimental environment where the perturbation voltage is input through a transformer, and the only difference between the results of Step 1 and Step 2 would be the impedance of the transformer itself.

Step 3:

In Step 2, the reference voltage source was a low impedance power supply like an infinite bus. However, small power supplies connected to the microgrid (MG) are affected by the perturbations. Therefore, the infinite bus should be replaced with other distributed power sources (such as GFM inverter power sources, synchronous generators, etc.). In this project, due to the LA period and complexity of changing the system configuration, an inductor will be inserted at the output terminals of the stiff grid to simulate a low SCR (short circuit ratio) power source.

In this stage, it is expected to find the resonance frequency of the two-machine system (weak grid and the inverter). Furthermore, the change in natural frequency can be found from the difference in impedances by changing the control variables of the converter, PWM frequency, filter constants, etc.

3.1.2. Used standards

In these tests, we do not adopt specific standards.

3.1.2. Used procedures

In this program, the power amplifier (EGSTON, 200 kVA, 400 V) is used as an infinite bus source. EGSTON is usually used as a power amplifier for HIL (Hardware in the Loop) simulations by OPAL-RT. Because the HIL program is not used in this program, EGSTON is used as a programmable AC power supply, and the output command values of it are created by its real-time simulation software (RT-LAB). RT-LAB is a SCADA (Supervisory Control and Data Acquisition) that controls and measures data from laboratory-wide experimental equipment.

As power sources other than EGSTON, inverters (60 kVA, 400 V) and converters (60 kVA, 400 V) created by SINTEF are used. The inverter can be controlled either conventional GFL and GFM (VSM) controls, which were created by SINTEF [Suul, D'Arco, Guidi, 2016]. The converter is used in BTB (Back-to-Back) as a DC voltage source for the above inverter.

Following are the procedures used in this program.

Step 1:

✓ Connect the inverter and the perturbation source (EGSTON). Here, switching frequency of the inverter is 7 kHz, and EGSTON has both functions of making a perturbation voltage and a reference voltage.

✓ Input an output command from RT-LAB to EGSTON. The command is a composite signal of reference (50 Hz, 400 V_{LL}) and perturbation voltages (0.5 to 5 kHz, 10 V_{LL}). This configuration is the current perturbation injection for an equipment that operating stand-alone.

✓ Three of the six output ports of the EGSTON are used to output a composite AC voltage of reference and perturbed voltages. Two of the remaining three ports are used as the DC voltage source for the inverter.

✓ Measure the voltages and currents at the gate/power source sides of the inverter, respectively, and calculate their dq impedance matrices in the rotating frames. The output filter between the two measurement points consists of an LCL filter (Reactance of the gate side: $L_1 = 0.5\ mH$, Capacitance: $C = 50\ \mu F$, Reactance of the source side: $L_2 = 0.2\ mH$).

Step 2:

✓ Make three single-transformers for the voltage perturbation injection. Adjust the winding ratio so that the ratio of primary to secondary voltage is around 10:1.

✓ The primary side of the transformer is connected to EGSTON using the three of the six output ports of the EGSTON, which is used only for the perturbation voltage generation (0.5 to 5 kHz, 2-100 V_{LL}).

✓ The secondary side of the transformer is inserted in series between the source (EGSTON) and the load (inverter). EGSTON is also using the remaining three output ports, and generate the reference voltage (50 Hz, 400 V_{LL}).

✓ To avoid magnetic saturation of the transformer and large current flow, the applied voltage is reduced as the frequency decreases in the frequency range below the commercial frequency.

Step 3:

✓ An inductor, meaning the power supply impedance, is inserted at the output terminal of EGSTON, to simulate a low SCR. Then, input a perturbation voltage as same as in the Step 2.

✓ Measure the voltages and currents and calculate the dq impedance matrices as same as in the Step 2.

✓ Check how the perturbation voltage acts on the sub-system on both sides of the transformer and how the stability of overall system is changed compared to Step 2.

✓ Check the differences in impedances by varying the inverter control parameters.
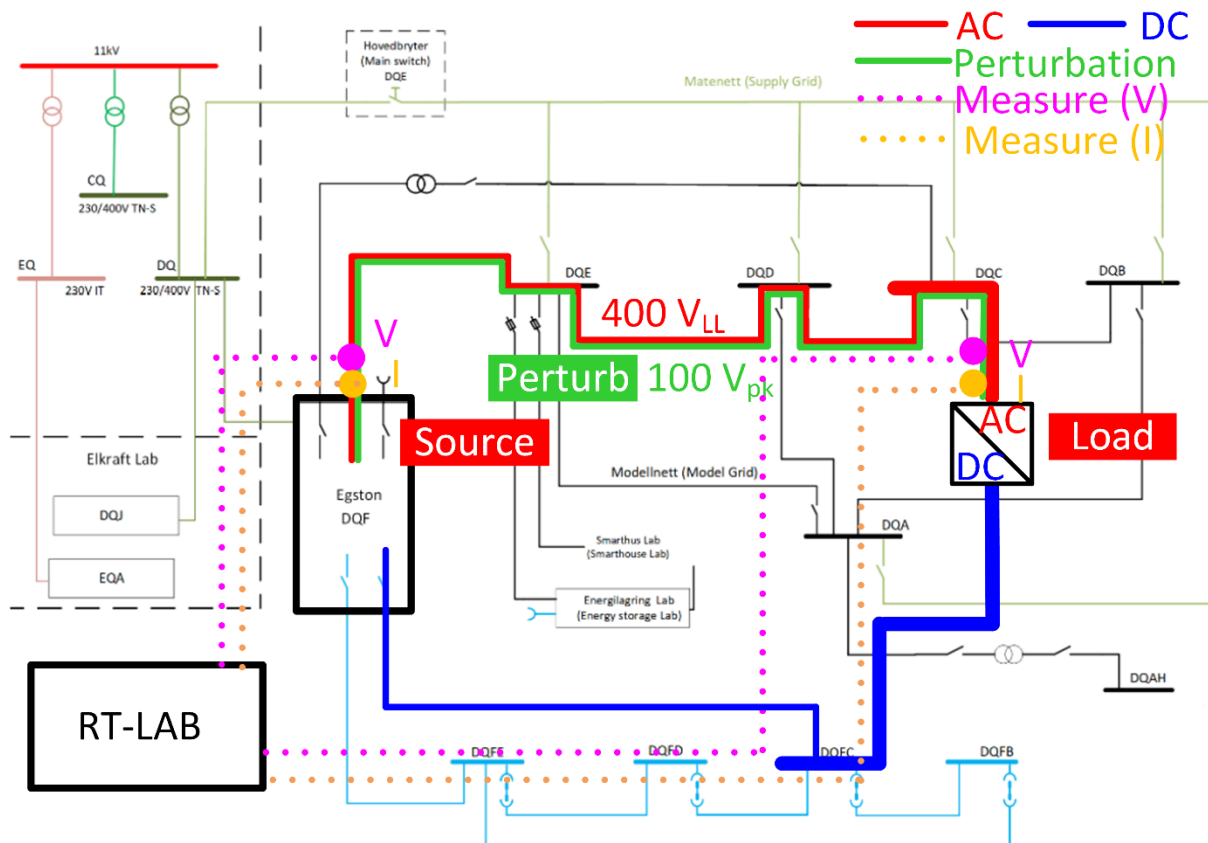
3.2 Test Set-up(s)

3.2.1. Step 1

Figure 1: Configuration of the test system in Step 1.

Figure 1 shows a configuration of the test system in Step 1 [SINTEF, 2020]. Cables/wires and communication lines are depicted in the solid and dot lines, respectively. AC (reference), AC (perturbation), and DC voltages are red, green, blue lines, respectively, and measured voltages and currents are pink and orange, respectively.

The measured signals are the voltages and currents at the output terminals of EGSTON

(source: 200 kVA) and the inverter (load: 60 kVA), respectively. Here, the inverter (load) voltage and current are measured at the gate side of the output filter.

Sequencing operations for system startup and shutdown are performed from the SCADA (RT-LAB) system, and data is measured every 100 us (which is the maximum sampling frequency) by this SCADA.
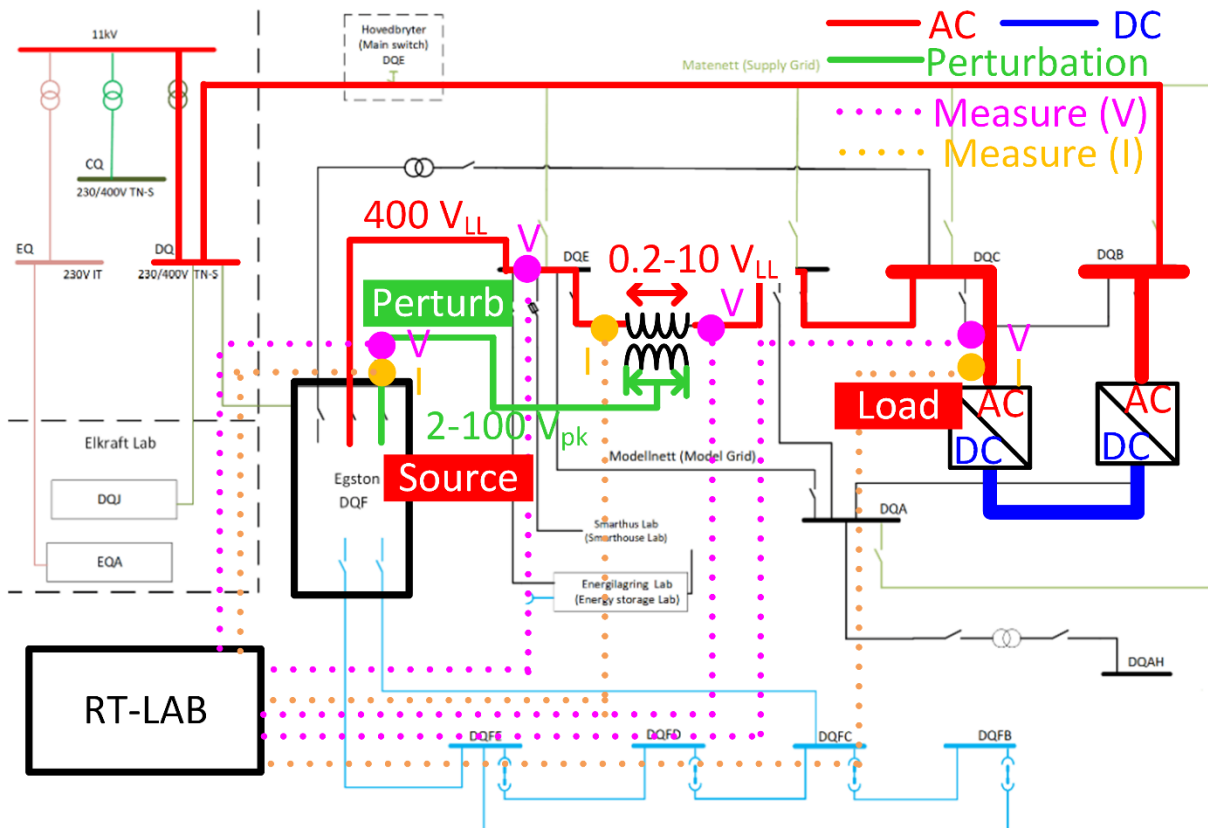
3.2.2. Step 2

Figure 2: Configuration of the test system in Step 2.

Figure 2 shows a configuration of the test system in Step 2. The difference from Step 1 is that the voltage output from EGSTON is divided into a reference signal and a perturbation signal. Other difference from Step 1 is that the secondary of the transformer is inserted in series between busbars of DQE and DQD, and the reference and perturbation voltages output separately from EGSTON are applied as the source-side phase voltage of the secondary transformer and the drop voltage of the primary transformer.

With this change, the voltage and current to be measured at the EGSTON terminals are the perturbation voltage and perturbation current applied to the primary transformer. Therefore, in order to measure the influence of the reference voltage of each of the two sub-systems from the perturbation voltage, the source and load side voltages of the secondary transformers and the current flowing through it are additionally measured. As in Step 1, the difference between the voltage measured at the load side of the secondary transformer and the voltage measured at the inverter is the voltage drop due to the output filter.
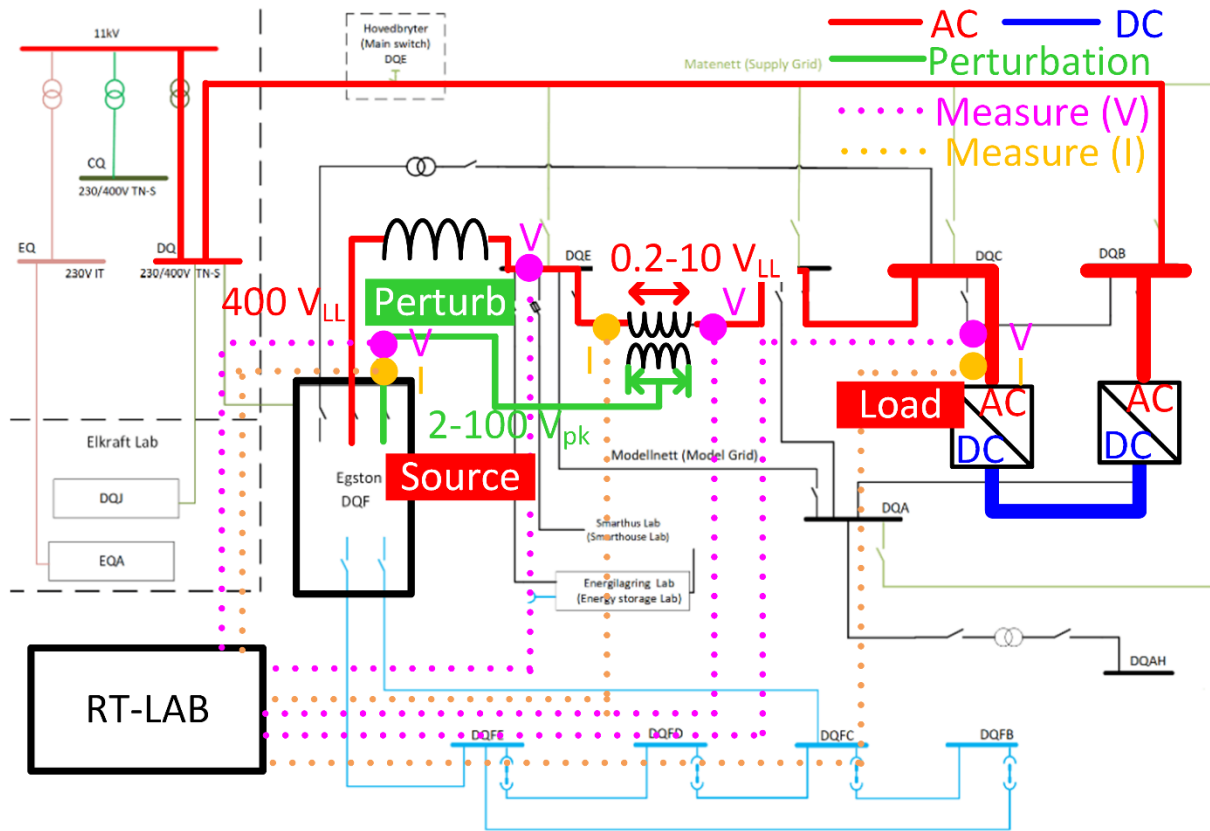
3.2.3. Step 3

Figure 3: Configuration of the test system in Step 3.

Figure 3 shows a configuration of the test system in Step 3. An inductor, meaning the power source strength, was inserted at this output terminal to simulate a low SCR.

3.2.4. Equipment used in the tests

The following figures show the equipment used in the experimental tests.

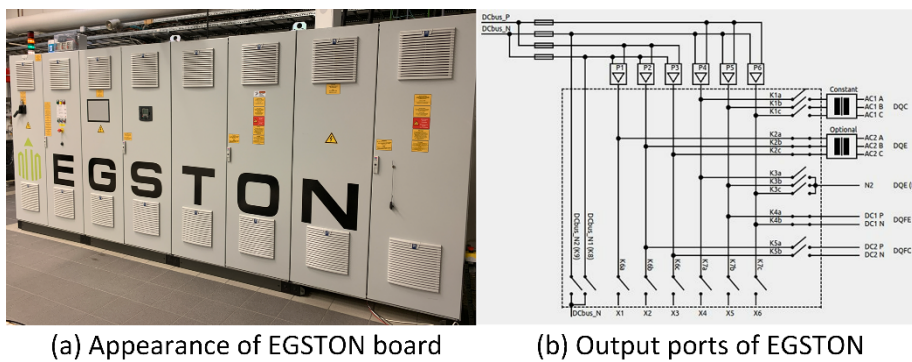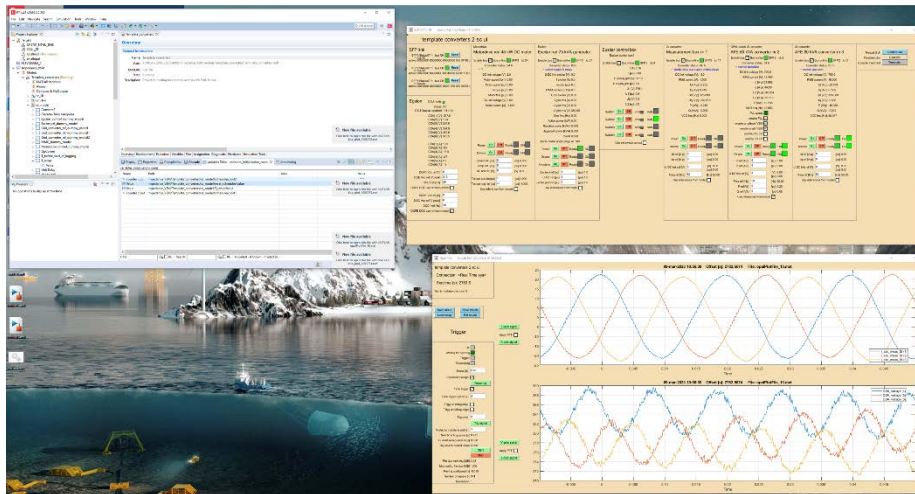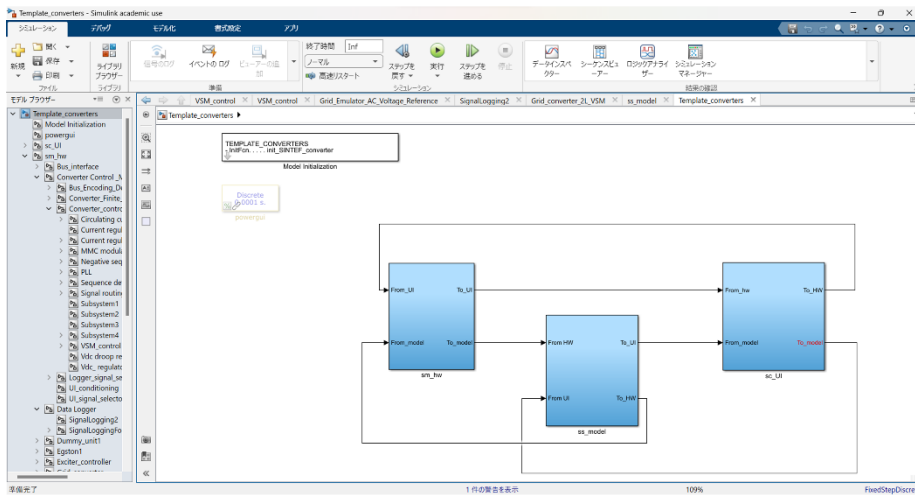(a) Appearance of EGSTON board   (b) Output ports of EGSTON

Figure 4: Power Amplifier (Programmable power source): EGSTON.

(a) SCADA interface of RT-LAB

(b) Program circuit of RT-LAB using Simulink interface

Figure 5: RT-LAB for output commands to EGSTON and data measurement.

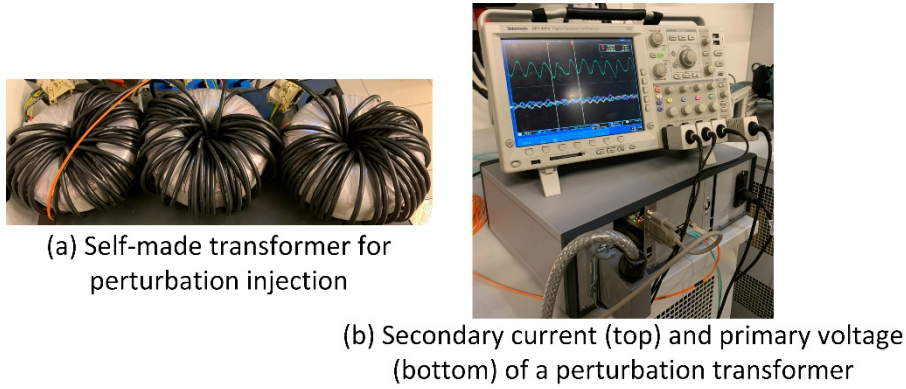*Figure 6: Inverter (left) and converter (right).*

(a) Self-made transformer for
perturbation injection

(b) Secondary current (top) and primary voltage
(bottom) of a perturbation transformer

Figure 7: Transformers for the series voltage injection.
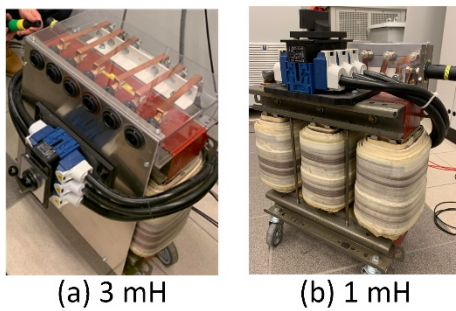

(a) 3 mH   (b) 1 mH

Figure 8: Three-phase inductors for the additional system impedances.

3.3   Data Management and Processing [Rygg A. , 2018]

3.3.1. Perturbation signal output from EGSTON

1. The output voltages from EGSTON are programmed by SCADA (RT-LAB). Equation (1) is the output command input to EGSTON from SCADA in Step 1. This is the equation for perturbation input to the d axis (v_d), but the same applies for input to the q axis. To convert a three-phase signal on stationary reference frame to a two-axis signal on synchronous reference frame, two independent signals are needed. (The d and q axes are orthogonal and independent.)

Here, A is the perturbation voltage amplitude of ± 20 (V) and ω_p [rad/s] is the perturbation angular velocity. $v_{ref} = 310$ (V) is a wave amplitude of a reference phase voltage (instantaneous value), which means that the line-to-line voltage is 400 (V_{LL}) considering the amplitude of the perturbation (A).

$$v_d = v_{ref} + A sin(\omega_p t). \cdots\cdots\cdots\cdots\cdots\cdots\cdots\cdots\cdots\cdots\cdots\cdots\cdots\cdots \text{(1)}$$

In Steps 2 and 3, v_d is divided into 2 parts: reference voltage ($A = 0$) and the perturbation voltage ($v_{ref} = 0$). Because a perturbation voltage of 50 Hz in synchronous reference frame indicates a DC voltage in stationary reference frame, the amplitude of the perturbation (A) input via the transformer is set as in Equation (2).

$$|A| = \left(\omega_p - 2\pi 50\right) * 4 \quad when\ 2\pi 25 < \omega_p < 2\pi 75,$$

$$|A| = 100 \qquad\qquad\qquad when\ \omega_p \le 2\pi 25\ or\ \omega_p \ge 2\pi 75. \cdots\cdots\cdots\cdots \text{(2)}$$

3.3.2. Processing of the measured signals

1. Measure the time responses (instantaneous values) of voltages and currents at the point where the impedance is required. The measurement time is 3 perturbation periods under 3 Hz or 1 s over 3 Hz after system settling, and the sampling frequency is 10 kHz, which is the maximum frequency of the data acquisition of SCADA (RT-LAB).

2. Discrete Fourier transformation (DFT) is applied to convert the measured data from time-domain to frequency-domain. The instantaneous phase is calculated from the converted fundamental component (50 Hz) data. This means the initial phase of the measurement data, and the phase of each discrete measurement data is calculated under the assumption that its frequency is constant at 50 Hz.

3. Using each discrete measurement data and their phases, transform the data from the stationary reference frame to the synchronous reference frame. DFT is applied to the data in the synchronous reference frame again. The signal on the synchronous reference frame contains the fundamental and perturbed wave components on the stationary reference frame as a DC component and a 50 Hz shifted frequency component. Then, the gain and phase of the perturbed signal components of the voltage and current, respectively, in synchronous coordinates are obtained.

3.3.3. Calculating the impedances

1. At each perturbation frequency, construct 2x1 vectors of voltage and current, respectively. Using the two 2x1 vectors for perturbations on the d- and q-axes, construct 2x2 matrices for voltage and current (V, I).

2. At each perturbation frequency, the impedance matrix (Z) or admittance matrix (Y) is calculated from V, I according to Ohm's law.

3. Only one impedance matrix is obtained in Step 1, while in Steps 2 and Step 3, two impedance matrices on both sides of the perturbation point (transformer).

### 3.3.4. Calculating the loop gain and the Nyquist plot

1. The loop gain matrix is defined as the product of the impedance and admittance matrices measured on either side of the perturbation injection.

2. To apply the generalized Nyquist criterion, two eigenvalue loci of the loop gain matrix are obtained.

3. The frequency of the trajectory closest to point (-1, j0) is required. Since the trajectory is a discrete sequence of points per perturbation frequency in the complex plane, the trajectory must be identified by a mathematical formula.

4. To ensure that the trajectory is placed as smoothly as possible, the perturbation frequency is varied more finely in regions where the phase changes significantly, and the process from impedance calculation to drawing the eigenvalue trajectory is repeated and added.

4   Results and Conclusions

4.1   Results

4.1.1. Step 1

Figure 9 shows the inverter impedance calculated in Step 1. The impedance is represented by a 2x2 matrix on dq-synchronous coordinates, with dd, dq, qq, qd impedances (scalars) clockwise from the upper left element. The inverter was equipped with VSM control, a type of GFM control. Figures 9(a) and 4(b) show the impedances of source and gate sides of the inverter, respectively. Figure 9(a) (source side of the inverter) includes the impedance of the output filter of the inverter; Figure 9(b) (gate side of the inverter) does not. The data were measured at 20 points of frequencies in the band from 0.1 Hz to 5 kHz on the logarithmic coordinate, divided into 100 equally.
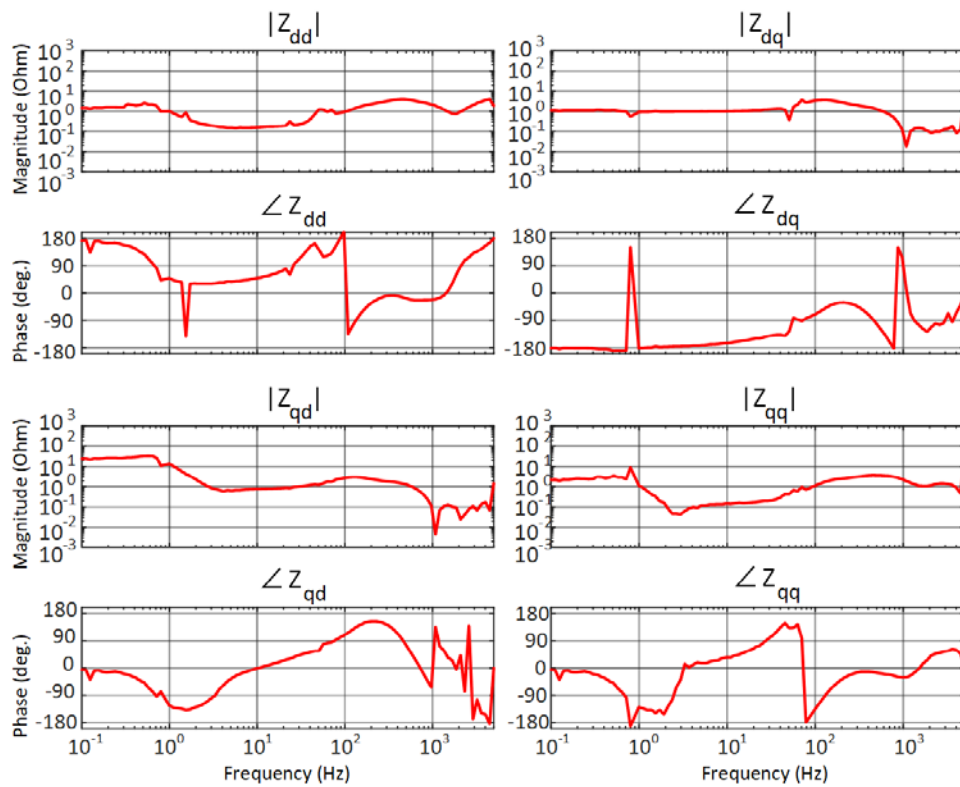
(a) Inverter (VSM) impedance of the power source (EGSTON) side in Step 1.
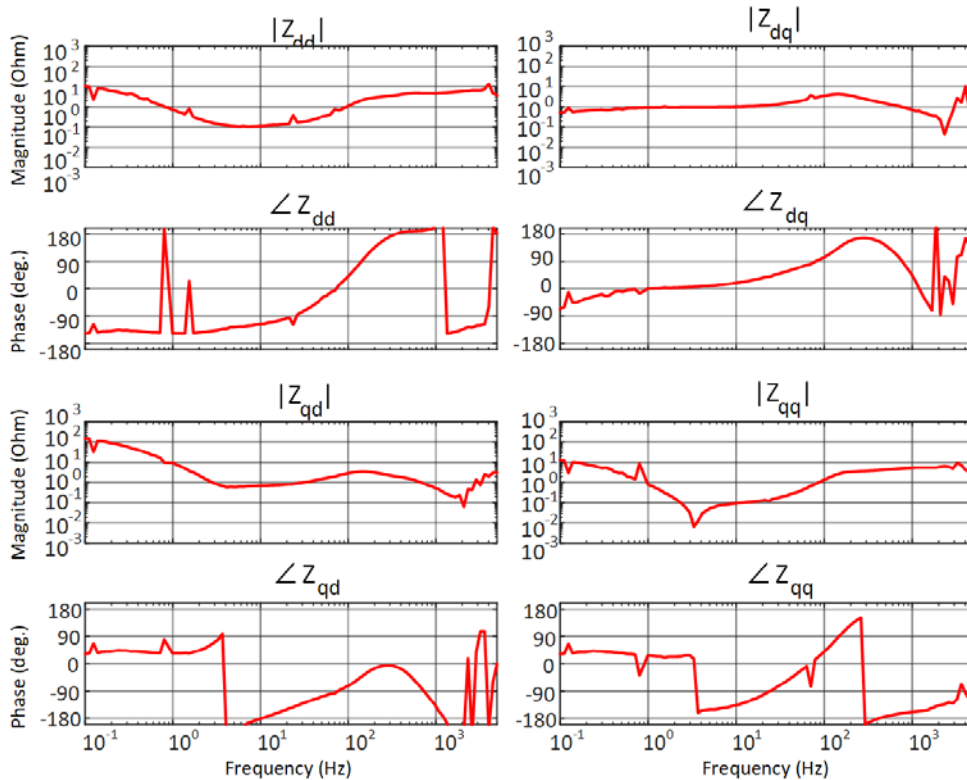
(b) Inverter (VSM) impedance calculated on the gate side in Step 1.

Figure 9: Inverter (VSM) impedance in Step 1.

Comparing the gain graphs in Figures 9(a) and 9(b), the difference in the low frequency band below 1 Hz can be observed and considered to represent the interference between the inverter control and the perturbation.

Also, when the perturbation frequencies were 50 Hz and 300 Hz, the impedances of both graphs fluctuated. The increase of the impedance on the synchronous reference frame at 50 Hz and 300 Hz can be caused by the 0 Hz (DC offset) and 250 Hz (5th harmonics) components on the stationary reference frame, respectively.

In the band above 1 kHz of Figure 9(b), the fluctuations were observed that may represent interference between the output filter and the perturbation. However, in the band above 1 kHz, not only is the signal attenuated by the output filter of the inverter, whose cut-off frequency is 1 kHz, but the sample frequency of the RT-LAB (10 kHz) determines the upper limit of the analysable frequency (5 kHz). In other words, it should be noted that the accuracy of the results in the high frequency band may be insufficient.

Therefore, the time response of the measured signal when the voltage contains high-frequency perturbations was checked. Figure 10, the signals measured at the gate side when the perturbation frequency was 5 kHz, shows that the signal waveform is highly distorted from a sinusoidal waveform. Therefore, measures such as increasing the sampling frequency or extending the sample time will be necessary to improve the accuracy of the impedance calculation in a high frequency band. Furthermore, the red arrow in Figure 10 shows a slight offset of the currents in the synchronous reference frame, and the yellow arrow shows the 300 Hz component included in the i_q current.
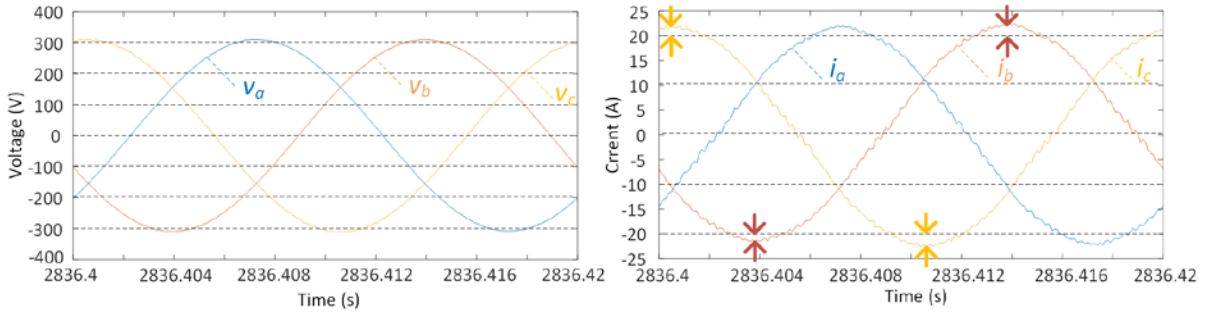
(a) Measured signals in the stationary reference frame at the gate side in Step 1. Perturbation frequency was 5 kHz.
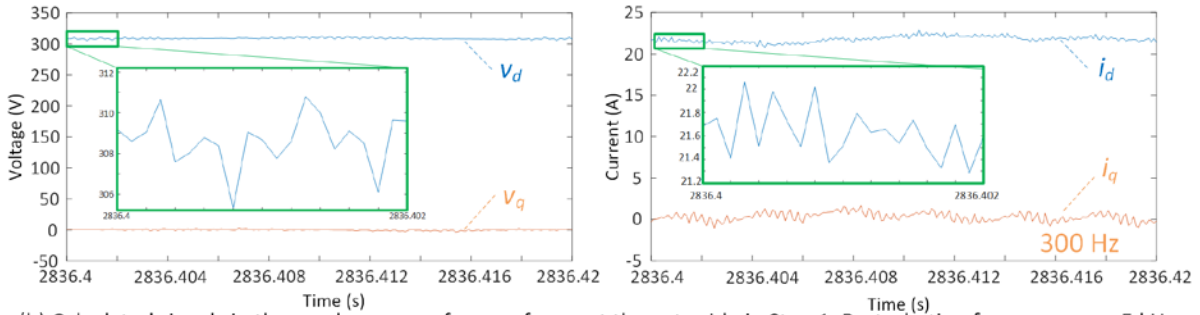
(b) Calculated signals in the synchronous reference frame at the gate side in Step 1. Perturbation frequency was 5 kHz.

Figure 10: Measured signals in the stationary reference frame (a) and the calculated signals in the synchronous reference frame (b) at the gate side in Step 1. The perturbation frequency was 5 kHz.

4.1.2. Step 2

Figure 11 shows the impedances on the synchronous reference frame on both sides of the transformer when a series voltage perturbation is injected in the middle of the system consisting of EGSTON and a GFM (VSM) inverter. Figures 11(a) and 11(b) show the impedances of the grid EGSTON and VMS sides of the injection transformer.

The green line in Figure 11(b) is the result of Step 1 (Figure 9(a)). In Step 2, the number of points was increased at the perturbation frequency where the impedance changed strongly in Step 1 (80 sampling points were added around 50 Hz and 100 sampling points were added in the high frequency band above 1 kHz) to improve the accuracy over the Step 1 results.

In Figure 11(b), the green and red lines are in good agreement, indicating the validity of the perturbation voltage injection test results using a series transformer.

From Figures 11(a) and 11(b), It can be confirmed that the impedance of the infinite bus is much smaller than that of the invert-er. However, in the band of ±25 Hz centred at 50 Hz on the synchronous reference frame, the accuracy of the results is considered insufficient because the amplitude of the perturbation signal was set to be small, as in Equation (2). Furthermore, similarly as in Step 1, it should be noted that the signal is attenuated by the inverter's output filter in bands above 1 kHz, and the RT-LAB's sample frequency limit reduce the accuracy of the results.
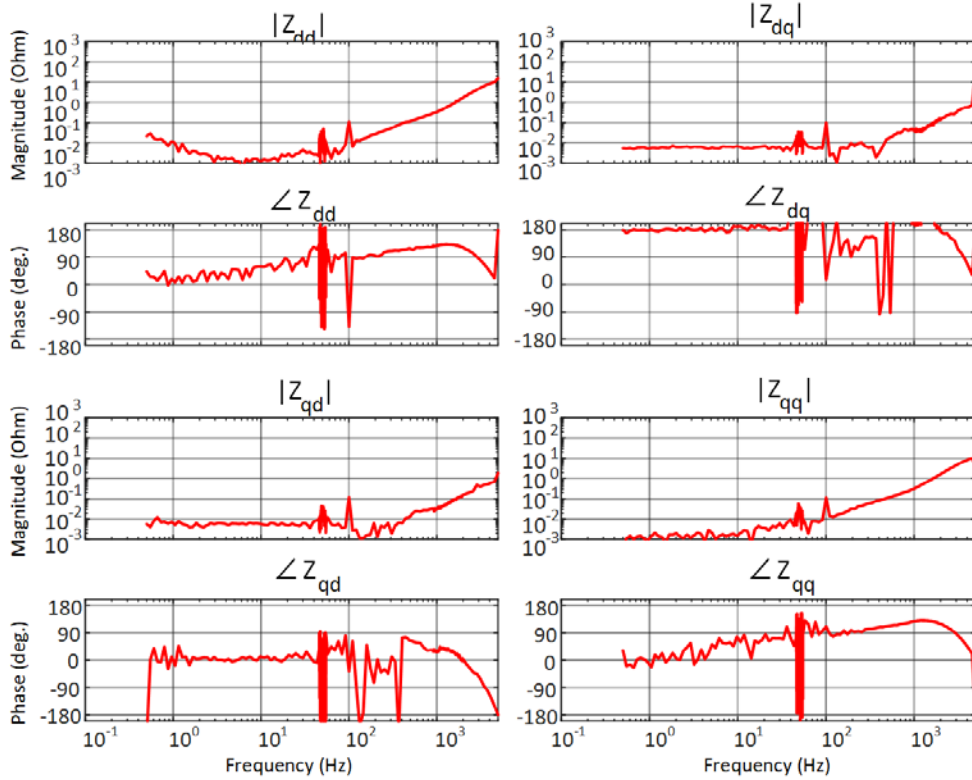
(a) Grid (EGSTON) side impedance of the injection transformer in Step 2.
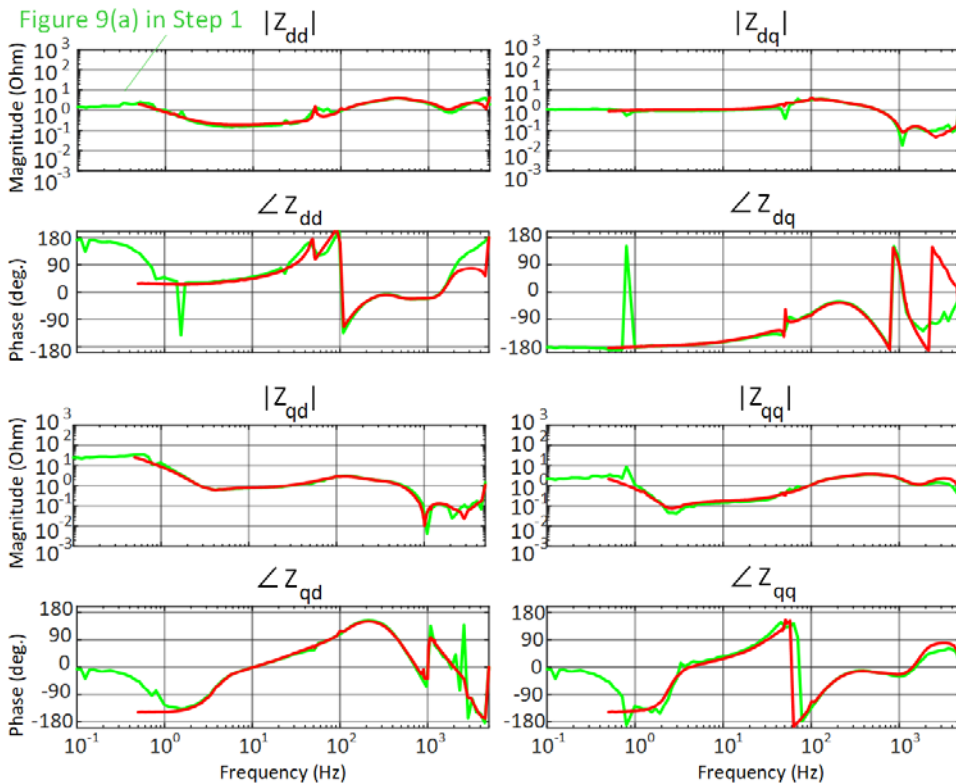
(b) Inverter (VSM) side impedance of the transformer in Step 2.

Figure 11: Grid (EGSTON) and Inverter (VSM) impedances in Step 2.

4.1.3. Step 3

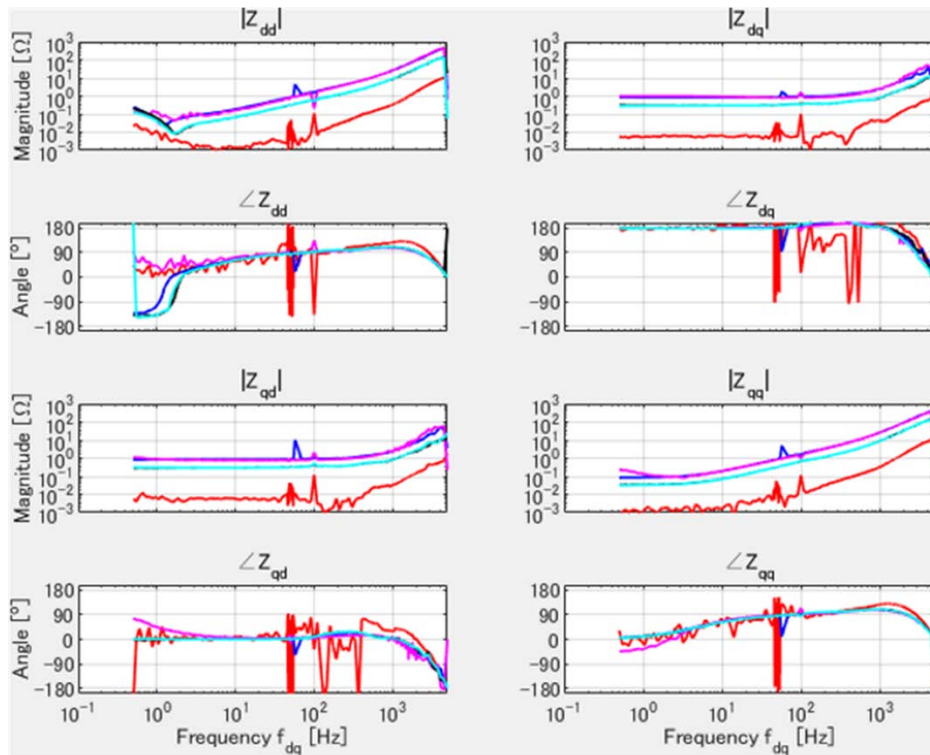*Table 1: Test cases used in Step 3.*

	Control methods of the inverter (GFL/GFM)	Power flow (Generation/ consumption)	Inductance of the additional inductor	Rate of change of perturbation amplitude around 50 Hz	
				d-axis	q-axis
#1 (magenta)	GFL	Generation	3 mH (SCR: 2.83)	4 V/Hz	2 V/Hz
#2 (blue)	GFM (VSM)	Generation	3 mH (SCR: 2.83)	4 V/Hz	4 V/Hz
#3 (black)	GFM (VSM)	Generation	1 mH (SCR: 8.49)	4 V/Hz	4 V/Hz
#4 (light blue)	GFM (VSM)	Consumption	1 mH (SCR: 8.49)	4 V/Hz	4 V/Hz

In this step, four types of tests were conducted. Table 1 lists the test cases of the tests in Step 3. The colours in the table represent those in the test results (Figure 12). Changed parameters were the control methods of the inverter (#1(magenta) vs #2(blue)), the inductance of the additional inductor (#2(blue) vs #3(black)), and the power flow (#3(black) vs #4(light blue)).

Here, in test #1 using GFL control, a current exceeding the overcurrent threshold flowed when a 50 Hz q-axis perturbation voltage was injected. Therefore, the change rate and the maximum limiter of the amplitude of q-axis perturbation voltage around 50 Hz was reduced from 4 V/Hz to 2 V/Hz and 100 V to 50 V, respectively (Equation (3)).

$$|A| = (\omega_p - 2\pi50) * 2 \quad when \ 2\pi25 < \omega_p < 2\pi75,$$

$$|A| = 50 \quad when \ \omega_p \leq 2\pi25 \ or \ \omega_p \geq 2\pi75. \ \cdots\cdots\cdots \ (3)$$

(a) Grid (EGSTON) side impedance of the injection transformer in Step 3.

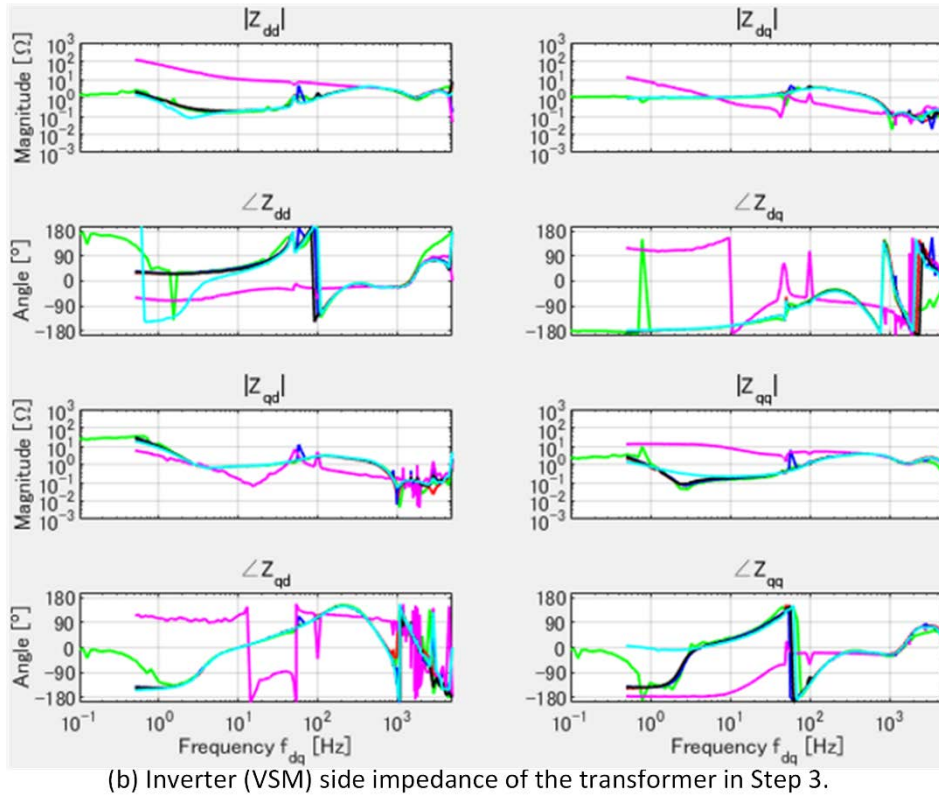(b) Inverter (VSM) side impedance of the transformer in Step 3.

Figure 12: Impedances of grid (EGSTON) and inverter (VSM) compared between test cases.

Figure 12 shows the impedances of grid (EGSTON) and inverter (VSM) compared between the test cases. The result of Step 1 (Figure 9(a)) is overlaid in green and the results of using the injection transformer without extra inductor in Step 2 (Figure 11) is overlaid in red.

In Figure 12(a), #1(magenta) and #2(blue) were overlapped and #3(black) and #4(light blue) were overlapped, respectively. The inductor was connected to the output terminal of EGSTON, and its effects were appeared in the EGSTON-side impedance. Reasonable results were obtained with increasing gain in the order of the red line in Figure 11, the black line in #3, and the blue line in #2.

On the other hand, given that the same hardware was used, the effect of the software should appear in the low frequency range, and indeed, as shown in Figure 12(b), the difference between the control methods of GFL (#1 (magenta)) and GFM (#2 (blue)) showed up in the band below about 300 Hz of the inverter-side impedance.

The comparison results of #3 (black) and #4 (light blue) represent the effect of power flow in the opposite direction, which is also shown in the impedance on the inverter side. In the low frequency band of the dd and qq elements of the impedance matrix, not only the phase inverted by 180 deg, but differences in gain were also appeared, representing differences in the charging and discharging characteristics of the inverter.

In the EGSTON side impedance in Figure 12(a), except for the red curve in Step 2 (Figure 11), there are frequencies in the 1 to 2 Hz band where the gain characteristics change significantly. Since a normal constant voltage source cannot change its characteristics in such a band, it seems that the effect of EGSTON's internal control is affected by the inverter when the output impedance is high. This needs to be clarified in more detail in the future.

4.2 Evaluation of system stability

As mentioned in section 3.3, to evaluate the stability of the system, it is necessary to calculate the impedance ratio (loop gain matrix) of the left and right perturbation injection points and study their two eigenvalue trajectories.

Because the target system configuration in this program was relatively simple, the number of measurement points was sufficient to display the eigenvalue loci in the linear complex domain; however, if the target circuit is more complicated, the number of measurement points may be insufficient, especially in the high frequency band.

By setting each direction from the perturbation injection point to the EGSTON or inverter the positive direction of the current, the system may become unstable at the gain intersection frequencies where the phase margins are close to zero.

4.2.1. Comparison of inverter control (Step 2 vs #1 of Step 3)

Figures 13(a) and 13(b) show the overlayed impedances on the left and right (EGSTON and INV) sides of the perturbation points in Step 2 and #1 of Step 3, respectively. Figures 14(a) and 14(b) show the eigenvalue (λ_1, λ_2) loci of the loop gain matrices of Step 2 and #1 of Step 3, respectively. The intersection frequencies of the impedance gains with the possibility of instability are roughly, but not exactly, consistent with the frequencies that pass near the point (-1, j0) in the eigenvalue locus of the loop gain matrix.

In Step 2, gain intersections were observed in the range of 1.6 kHz to 1.8 kHz from Figure 13(a), but the system is stable because there is enough phase margin from Figure 14(a). Similarly in #1 of Step 3, a gain intersection was observed around 254 Hz from Figure 13(b), but the system is stable because there is enough phase margin from Figure 14(b).
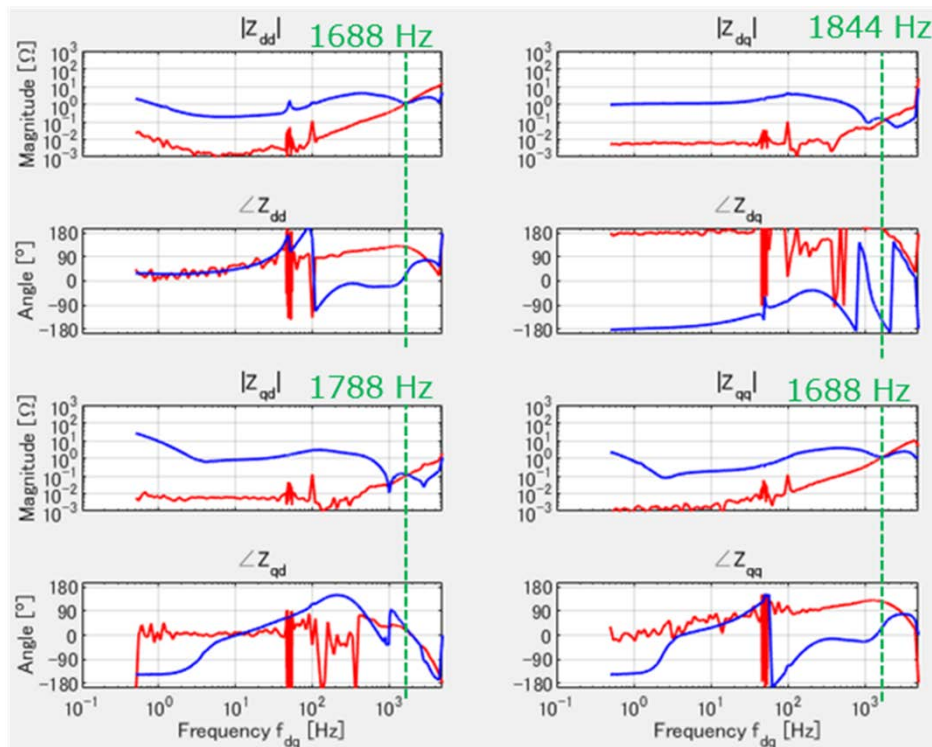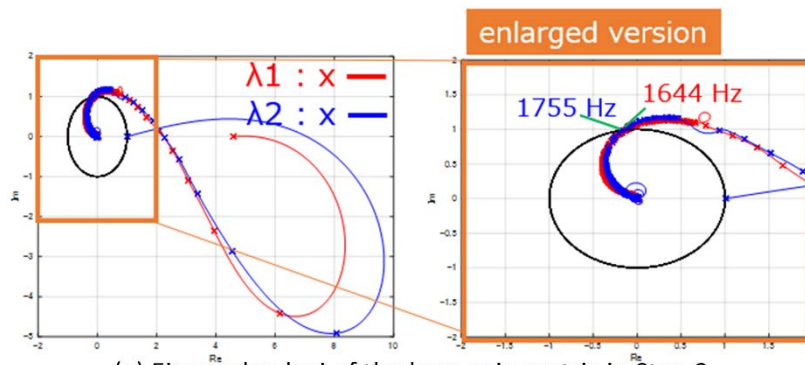

(a) Overlayed impedances of Grid (EGSTON) and GFM-inverter (VSM) in Step 2.
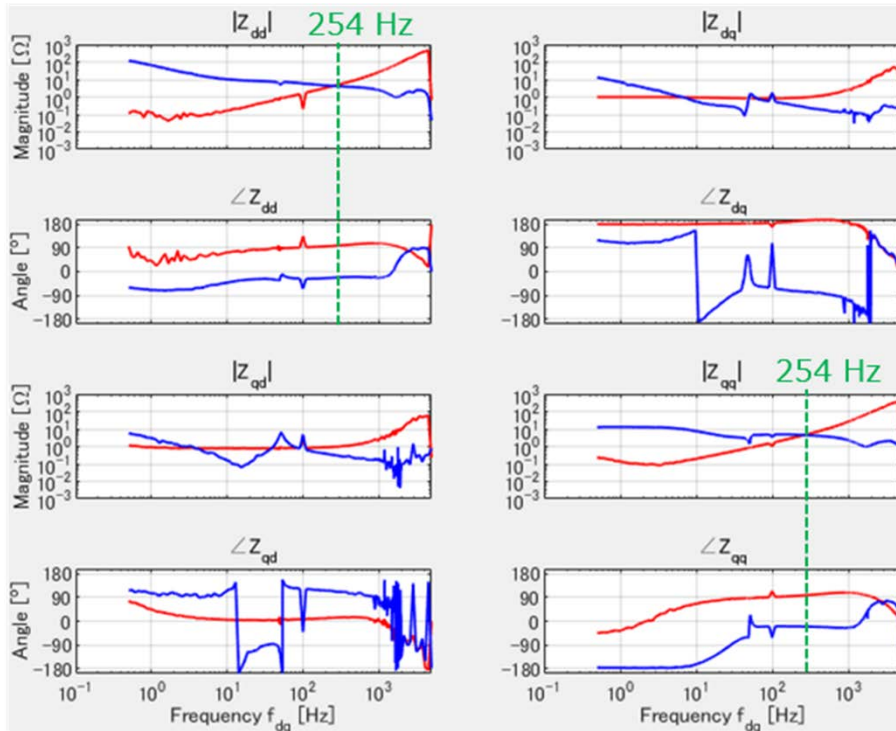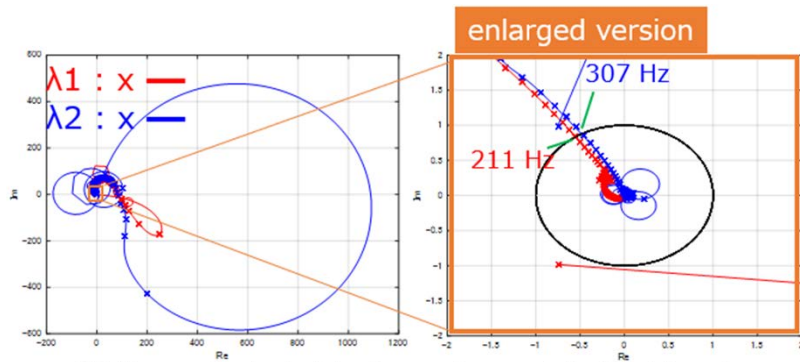
(b) Overlayed impedances of Grid (EGSTON) and GFL-inverter in # 1 of Step 3.

Figure 13: Overlayed grid (EGSTON) and inverter (VSM) impedances in Step 2 and #1 of Step 3.
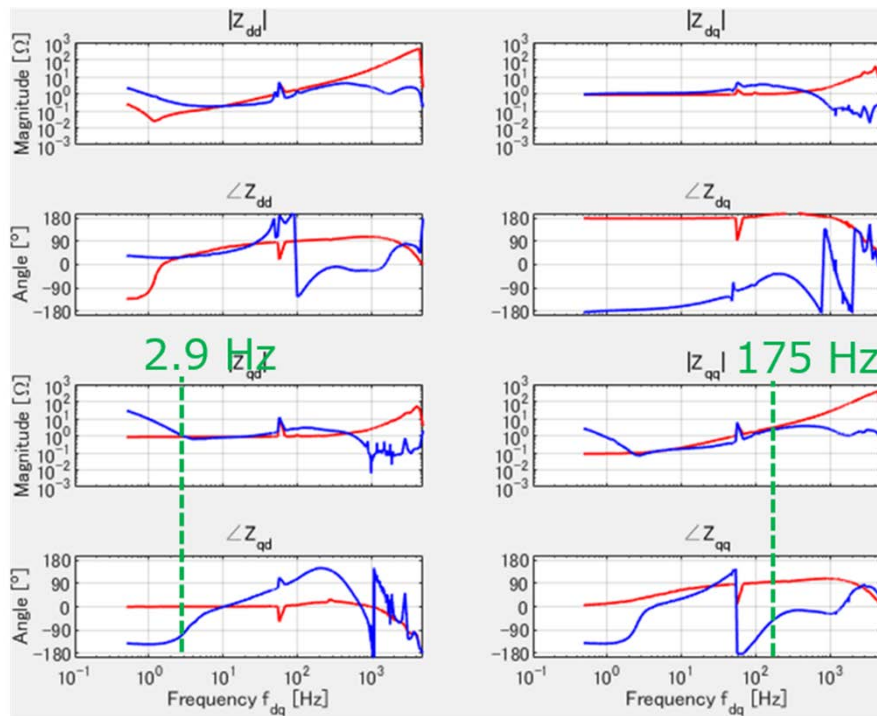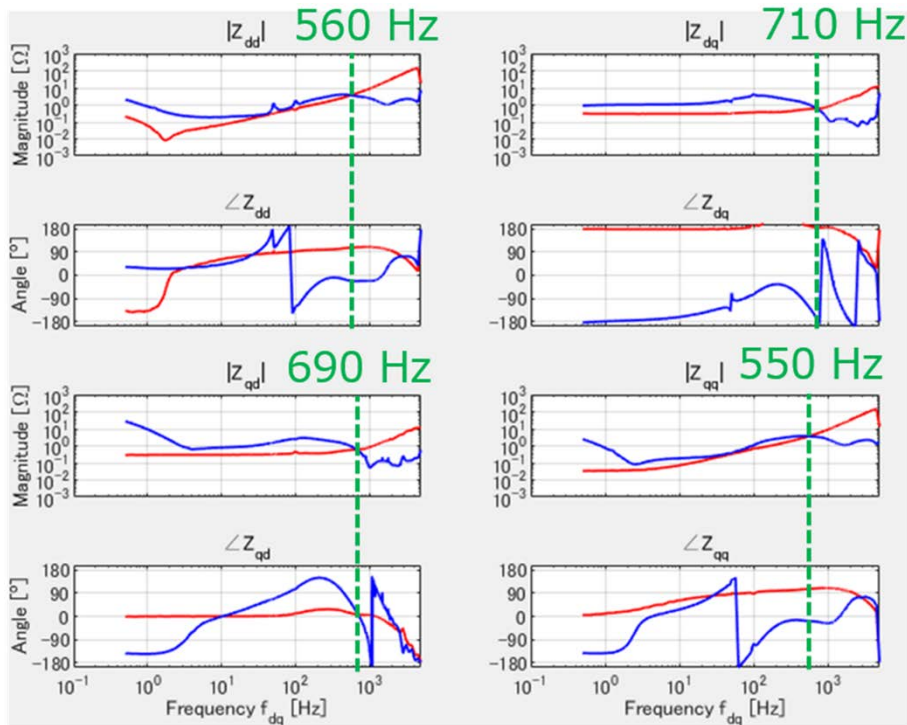

(a) Eigenvalue loci of the loop gain matrix in Step 2.

(b) Eigenvalue loci of the loop gain matrix in #1 of Step 3.

Figure 14: Eigenvalue loci of the loop gain matrix in Step 2 and #1 of Step 3.

4.2.2. Comparison of the inductance of the additional inductor (Step 2 vs #2 of Step 3 vs #3 of Step 3)

(a) Overlayed impedances of Grid (EGSTON) and GFM-inverter (VSM) in #2 of Step 3.

(b) Overlayed impedances of Grid (EGSTON) and GFL-inverter in # 3 of Step 3.

Figure 15: Overlayed grid (EGSTON) and inverter (VSM) impedances in #2 and #3 in Step 3.

(a) Eigenvalue loci of the loop gain matrix in #2 of Step3.

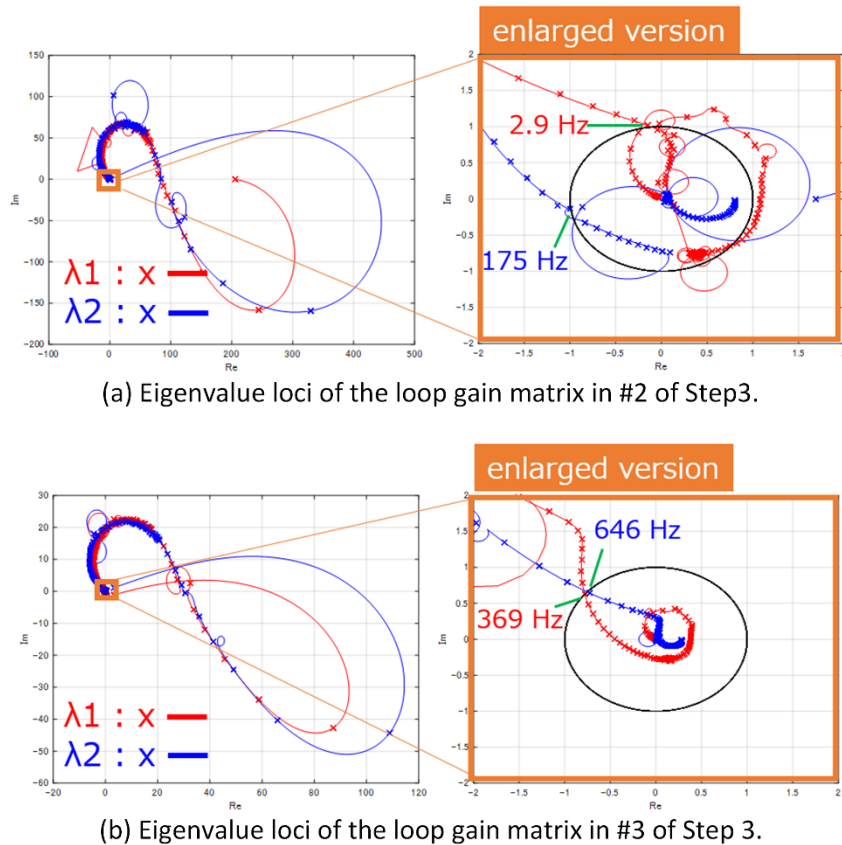(b) Eigenvalue loci of the loop gain matrix in #3 of Step 3.

Figure 16: Eigenvalue loci of the loop gain matrix in #2 and #3 in Step 3.

Next, the inverter was GFM (VSM) controlled at generation mode and the impact of the strength of the power source was compared. Figures 13(a), 15(a), and 15(b) show the results of overlaying the impedances on the left and right sides of the perturbation point with no (Step 2), 1mH (#3 of Step 3), and 3mH (#2 of Step 3) inductor connected to the output terminal of EGSTON, respectively.

As EGSTON's impedance gain curve, indicated by the red line, decreased in the order of Step 2, #3 of Step 3, and #2 of Step 3, the gain intersection frequency also decreased (for the qq element) to 1688 Hz, 550 Hz, and 175 Hz. Comparing the phase margin in Figure 14(a) (Step 2), Figure 16(b) (#3 of Step 3), and Figure 16(a) (#2 of Step 3), it is clear that Step 2 has a phase margin of approximately 90 deg at 1755 Hz and #3 of Step 3 has that of approximately 45 deg at 369 Hz, while #2 of Step 3 has almost no phase margin at 175 Hz.

What can be said from these results is that when the VSM inverter used in the test is connected to a weak power system, the system has poles around 175 Hz and is likely to become unstable when a disturbance in this frequency band is input.

If the grid impedance cannot be lowered to avoid the resonance, the affecting factors could be identified on the inverter side and the control and equipment parameters could be adjusted. This is an issue to be addressed in follow-up.

4.2.3 Comparison between the generation and consumption (#3 vs #4 of Step 3)

Grid-connected inverters that are equipped with energy storage devices in the DC section, such as VSM-controlled inverters, can charge (consume power) from the grid. Although the

only difference in inverter control is the reversal of the sign of the current, depending on the impedance and control of the storage device, there can be a significant difference in the charging and discharging characteristics of the interconnection point.

Figure 17 shows the results when the inverter is operated in consumption (charging) mode (#4 of Step 3). The impedance of the inductor at the EGSTON output terminal was set to 1 mH and is compared with #3 of Step 3, where the inverter was operated in the generation (discharge) mode under the same conditions.

As stated in Section 4.1.3, The difference in the characteristics of charging and discharging in the inverter is only seen in the low frequency band below 10 Hz, and the impedance gains of EGSTON and the inverter do not intersect in that band for either mode (Figures 15(b) or 17(a)). In both modes, the gain curves intersect at around 700 Hz. However, as seen in Figure 16(b) and Figure 17(b), there is enough phase margin and both systems were stable.
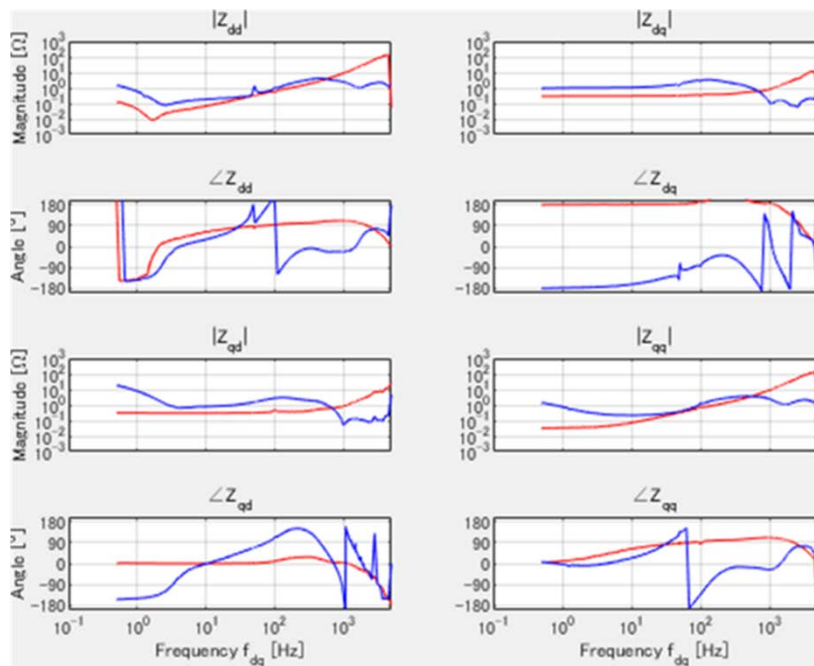
(a) Overlayed impedances of Grid (EGSTON) and GFL-inverter in #4 of Step 3.
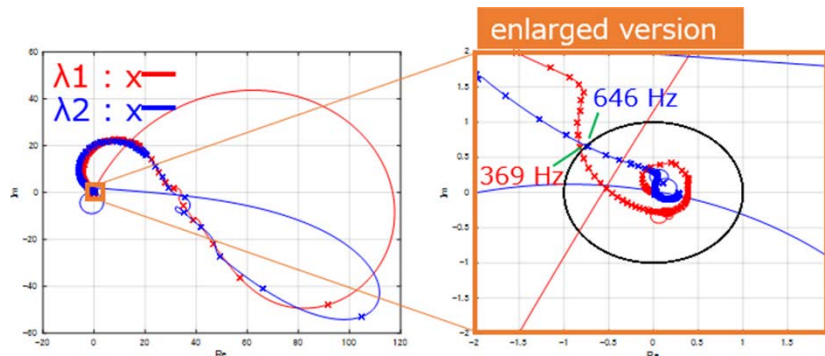
(b) Eigenvalue loci of the loop gain matrix in #4 of Step 3.

Figure 17: Overlayed grid (EGSTON) and inverter (VSM) impedances and eigenvalue loci of the loop gain matrix in #4 of Step 3.

4.3 Discussion

4.3.1. Different types of perturbations

In this program, impedance was measured by injecting voltage perturbations. When the inverter under investigation is connected to a constant voltage source, the injected perturbation voltage almost exclusively affects the inverter side. If the line impedance on the inverter side is relatively high compared to the power supply side, the current generated by the perturbation will also be small, making it difficult to measure the impedance on the power supply side.

On the other hand, when a current perturbation is injected, most of the perturbation current will flow to the power supply side, and since the line impedance of the power supply is usually very low, the potential difference generated by the perturbation becomes must be small, making it difficult to measure the impedance of the inverter side.

Impedance analysis is a technique to measure the left-right impedance balance by dividing or shunting the perturbation injected at the splitting point. When investigating low impedances such as constant voltage sources or inverters with extremely large impedances, it is necessary to confirm the validity of the calculated values.

4.3.2. Signal strength for voltage perturbation

Figure 18 shows the amplitudes of the measured signals in the test cases of Step 2, #2 and #3 of Step 3. Figures 18(a) and 18(b) in the upper row show the results when the vd perturbation was injected, and Figures 18(c) and 18(d) in the lower row show the results when the vq perturbation was injected. Figure 18(a) and Figure 18(c) in the left column represent the d-axis components of the measurement signal, and Figure 18(b) and Figure 18(d) in the right column represent the q-axis components of the measurement signal. Each component contains the amplitudes of the three measurement signals and represents the EGSTON side voltage, inverter side voltage, and current from top to bottom.

The vertical axis range was expanded to match the magnitude of the signal in the low frequency band where no resonance occurs, because the resonant signal becomes large around 175 Hz in the test case #3 of Step 3, as discussed in section 4.2.2.

From Equation (2), in the low frequency band with a gain of 1, an ideal calculation ignoring noise should result in a perturbation voltage amplitude of 100 V on the power supply side and 10 V on the system side. From Figure 18, it becomes difficult to measure the voltage and current of the EGSTON in step 2, which simulates an infinite bus, in the low frequency band where the impedance on the inverter side becomes relatively large, as described in the previous section.
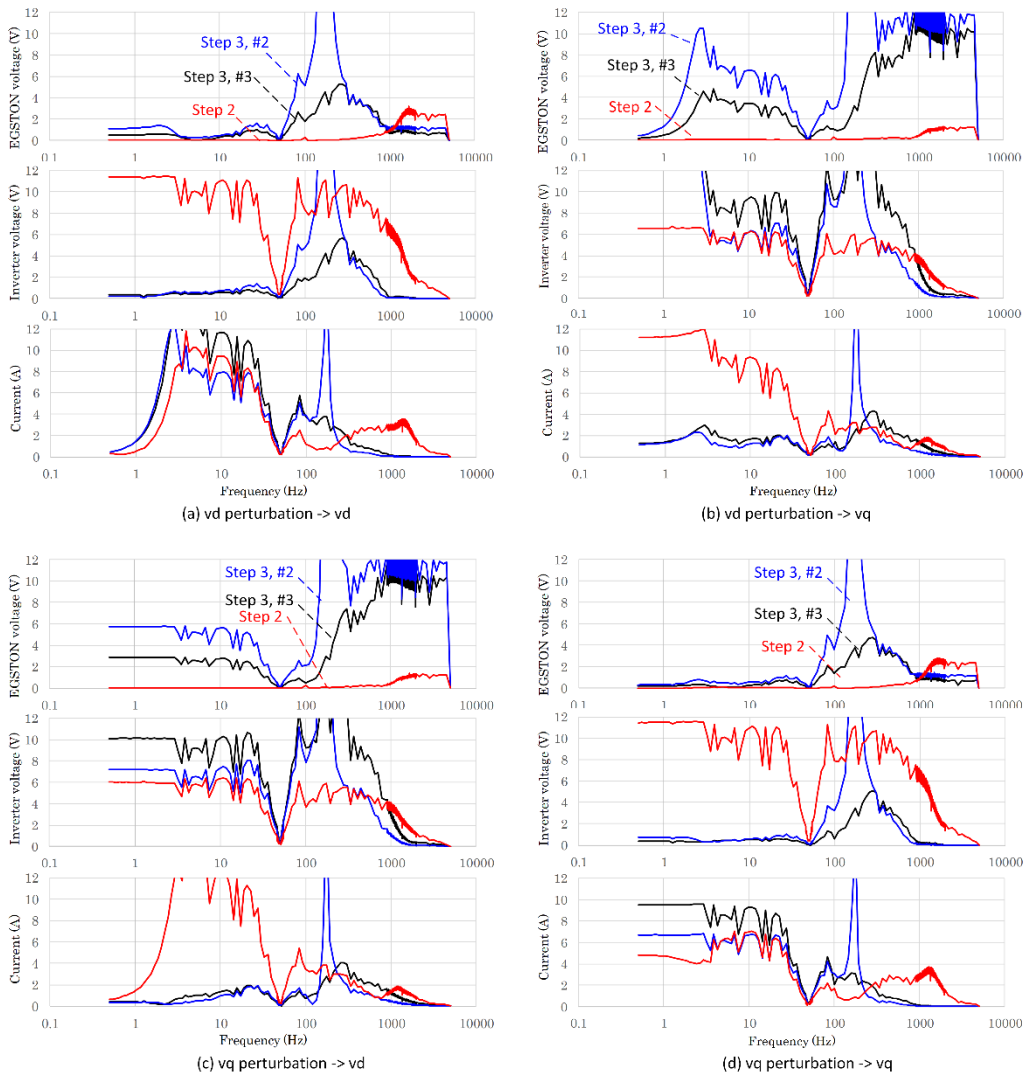
Figure 18: Comparison of the amplitudes of measured signals between test cases.

4.4 Conclusions

4.4.1 The impact of using the ERIGrid 2.0 LA programme

It is significant that program participants who do not own enough experimental facilities can use that provided by ERIGrid and obtain the data. It is also significant that researchers who have their own laboratories can expand the scope of their research with new objectives and uses.

4.4.2 The use of the HTD (Holistic Test Description)

In order to make meaningful use of the limited program period, adequate planning should be done prior to on-site experimentation. The HTD is useful as a guideline for this. However, because the availability of the actual equipment cannot be controlled by this project alone, and it is difficult to completely know the detailed connections and placements in advance. Then, not only using the HTD, but it is also necessary to proceed the experiment while planning together with the host at the site.

4.4.3 The multi-lab experiments

Program participants need to clarify what is missing and how far they can do pre-experimental tests with their own equipment, and from where they will start experimenting in the LA program. In addition, the collaboration will be maintained after the program is completed, making it possible to remotely process and jointly analyse data measured at multiple laboratories.

4.4.4 The Hardware-in-the-Loop (HIL) experiments

The HIL model was not used in this program, and the system was configured on a microgrid in the lab. In the future, the system could be extended by combining the HIL model, so that impedances of large systems, which are difficult to measure in practice, could be measured with a lab-scale mini-system.

In this case, in addition to measurement and calculation accuracy, the accuracy of the HIL model is required. The challenge is to obtain validity of the experimental results by consistency with mathematical and numerical (simulation) analyses.

5 Open Issues and Suggestions for Improvements

5.1 Laboratory Use Assignment

Because the host needs to use the laboratory for other research that is being conducted in parallel, it is necessary to coordinate the schedule for laboratory use. It is not uncommon for a laboratory to be unavailable due to an accident, and even in such cases, an alternative program should be prepared to make the most of the limited time available during the period.

In this program, however, sufficient time was allotted for laboratory use, and access was never restricted.

5.2 Necessary Expenses

Food, accommodations, and travel expenses will be reimbursed appropriately.

However, since communication costs are expensive, especially for students, it is expected that communication costs (cell phone) necessary for close cooperation with the host will also be compensated in the future.

In addition, the cost of procurement of equipment to be used only in the laboratory during the program (equipment purchased locally that cannot be used after the program ends) should be eligible for reimbursement.

References

Amin, M., & Molinas, M. (2016). *Self-synchronisation of wind farm in MMC-based HVDC system.* 2016 IEEE Electrical Power and Energy Conference (EPEC)*, 1-6.*

Amin, M., & Molinas, M. (2017). *Small-signal stability assessment of power electronics based power systems: A discussion of impedance-and eigenvalue-based methods.* IEEE Transactions on Industry Applications, Vol. 53, Issue 5*, 5014-5030.*

Belkhayat, M. (1997). Stability criteria for AC power systems with regulated loads. *Purdue University.*

Kiribuchi, T., Zaitsu, T., Doi, M., Kusaka, K., & Itoh, J. (2019). *Impedance-Based Stability Analysis of DC Bus System for Servo Drives.* 2019 21st European Conference on Power Electronics and Applications (EPE '19 ECCE Europe)*, 1-7.*

Middlebrook, R., & Cuk, S. (1976). *A general unified approach to modelling switching-converter power stages.* 1976 IEEE power electronics specialists conference*, 18-34.*

Ohuchi, K., Hirase, Y., & Molinas, M. (2022). *Impedance-Based Stability Analysis of Systems with the Dominant Presence of Distributed Power Sources.* 2022 International Power Electronics Conference (IPEC-Himeji 2022-ECCE Asia)*, 205-212.*

Rygg, A. (2018). Impedance-based methods for small-signal analysis of systems dominated by power electronics. *Trondheim: NTNU.*

Rygg, A., Molinas, M., Unamuno, E., Zhang, C., & Cai, X. (2017). A simple method for shifting local dq impedance models to a global reference frame for stability analysis. *arXiv preprint arXiv:1706.08313.*

Rygg, A., Molinas, M., Zhang, C., & Cai, X. (2017). *On the equivalence and impact on stability of impedance modeling of power electronic converters in different domains.* IEEE Journal of Emerging and Selected Topics in Power Electronics, Vol. 5, Issue 4*, 1444-1454.*

Shah, S., Koralewicz, P., Gevorgian, V., Liu, H., & Fu, J. (2021). *Impedance Methods for Analyzing Stability Impacts of Inverter-Based Resources: Stability Analysis Tools for Modern Power Systems.* IEEE Electrification Magazine, Vol. 9, Issue 1 *, 53-65.*

SINTEF. (2020). National Smart Grid Laboratory (SINTEF)*. Retrieved 3 7, 2023, from ERIGrid 2.0: https://erigrid2.eu/sintef/*

Sun, J. (2009). *Small-signal methods for AC distributed power systems–a review.* IEEE Transactions on Power Electronics*, 2545-2554.*

Suul, J., D'Arco, S., & Guidi, G. (2016). *Virtual Synchronous Machine-Based Control of a Single-Phase Bi-Directional Battery Charger for Providing Vehicle-to-Grid Services.* IEEE Transactions on Industry Applications, Vol. 52, Issue 4*, 3234-3244.*

Appendix A. Laboratory Access

A.1. Photos

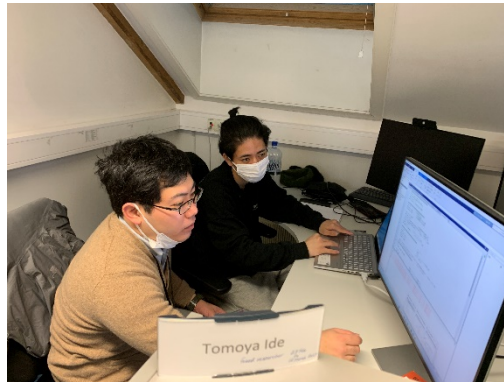*Figure 19: Students building the experimental apparatus.*

Figure 20: Students processing collected data.

Figure 21: Group photos (with SINTEF researchers).

A.2. Videos

Figure 22: Working Scene (Making of the perturbation injection transformer.)
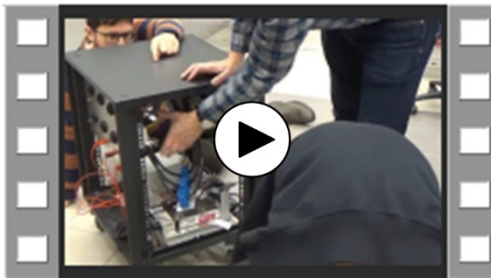

Figure 23: Working Scene (Connection of perturbation injection transformer to the power box.)

Disclaimer

This document contains material, which is copyrighted by the authors and may not be reproduced or copied without permission.

The commercial use of any information in this document may require a licence from the proprietor of that information.

Neither the Lab Access User Group as a whole, nor any single person warrant that the information contained in this document is capable of use, nor that the use of such information is free from risk. Neither the Lab Access User Group as a whole, nor any single person accepts any liability for loss or damage suffered by any person using the information.

This document does not represent the opinion of the European Community, and the European Community is not responsible for any use that might be made of its content.

Copyright Notice

© 2021 by the authors, the Lab Access User Group.